

Investigating deformations of RC beams: experimental and analytical study

Javier Ezeberry Parrotta^{*1a}, Hugo Corres Peiretti^{1a}, Viktor Gribniak^{2b,3}
and Alejandro Pérez Caldentey^{1c}

¹*Polytechnic University of Madrid, 28040 Madrid, Spain*

²*Vilnius Gediminas Technical University, 10223 Vilnius, Lithuania*

³*Institute of Polymer Mechanics, University of Latvia, Raina Blvd. 19, 1586 Riga, Latvia*

(Received February 15, 2014, Revised March 4, 2014, Accepted April 25, 2014)

Abstract. In this paper, a theoretical and experimental study of the sectional behaviour of reinforced concrete beams subjected to short-term loads is carried out. The pure bending behaviour is analysed with moment-curvature diagrams. Thus, the experimental results obtained from 24 beams tested by the authors and reported in literature are compared with theoretical results obtained from a layered model, which combines the material parameters defined in Model Code 2010 with some of the most recognized tension-stiffening models. Although the tests were carried out for short-term loads, the analysis demonstrates that rheological effects can be important and must be accounted to understand the experimental results. Another important conclusion for the beams tested in this work is that the method proposed by EC-2 tends to underestimate the tension-stiffening effects, leading to inaccuracies in the estimations of deflections. Thus, the actual formulation is analysed and a simple modification is proposed. The idea is the separation of the deflection prediction in two parts: one for short-term loads and other for rheological effects (shrinkage). The results obtained are in fairly good agreement with the experimental results, showing the feasibility of the proposed modification.

Keywords: reinforced concrete; moment-curvature; tension stiffening; beam growth; serviceability; shrinkage; eurocode 2; Model Code 2010; effective modulus of inertia

1. Introduction

The curvature analysis is a consolidated tool in current engineering practice, Ghali *et al.* (2012). For a reinforced concrete (RC) section the curvature express the inclination of the strain plane and is related to the deformations and deflections of linear elements as beams or columns.

Traditionally, the analysis related to RC elements where carried out neglecting the contribution of cracked concrete. However, nowadays, there is the consensus that tension-stiffening effects can

*Corresponding author, MSc. Structural Eng., E-mail: jie@he-upm.com

^aPh.D., E-mail: hcp@he-upm.com

^bPh.D., E-mail: viktor.gribniak@vgtu.lt

^cPh.D., E-mail: apc@he-upm.com

influence significantly the deformational behaviour of RC elements in the service range. A large number of publications confirm this fact, Bazant and Oh (1984), Vecchio and Collins (1986), Hsu (1996), Kaklauskas (2001) and Kaklauskas *et al.* (2011c), Gilbert (2007 and 2008), Bischoff (2008) and Balázs *et al.* (2013), among others.

In addition, rheological effects can have a considerable influence in the serviceability range introducing additional deformations, as indicated by Ghali *et al.* (2001) and Gilbert (2001). Shrinkage-induced camber occurs in asymmetrically-reinforced or cracked beams. On the other hand, creep increases the curvatures and the deflections.

The combined effect of shrinkage deformations and tension-stiffening was studied by Gilbert (2001); Bischoff (2001) and Kaklauskas and Gribniak (2011a). One of the most interesting effects is called “negative tension-stiffening”, as indicated by Gribniak (2009) and Zanuy (2010), which is produced by a release of compressive strains induced in the bar reinforcement by restraining shrinkage of concrete at the moment of cracking that hampers interpretation of the experimental measurements. This fact has to be assessed in order to obtain confident results of constitutive modelling. However, current design codes as EC-2 (2004) or ACI-318(2011) use interpolation equations empirically deduced from test data of shrunk RC elements and, therefore, the prediction models introduce the shrinkage effect in an integral manner. In some cases, this may lead to critical predictions of serviceability parameters (deformations or crack opening widths) of RC structures.

It can be stated that until now there is not a universally accepted tension-stiffening model, which can be applied with confidence in current professional practice. Thus, this paper is focused in the analysis of this problem combining experimental evidence and some of the most recognised analytical models. The major topics of the analysis carried out in this paper are:

- 1) Experimental study: deformation measurements and curvature analysis.
- 2) Influence of shrinkage on the experimental results.
- 3) Tension-stiffening models and their adequacy analysis.
- 4) Influence of the tension-stiffening effects on the curvature predictions.

2. Methodology

2.1 Numerical simulation procedure

The classical hypothesis used in serviceability (Ghali *et al.* (2012)) are a linear-elastic behaviour for steel in tension and compression and concrete in compression, neglecting the tensile strength (State II). On the other hand, the non-linearity for concrete, in compression, can be accounted by using the constitutive equation proposed by Sargin as proposed by Model Code 2010 (2012). However, in the serviceability range this equation does not significantly differs from elastic behaviour, at least up to a stress of $0.5f_{cm}$.

The tensile behaviour of concrete is the source of major uncertainties. In general, there are four main approaches to consider the tension-stiffening (Gribniak (2009)): 1) Stress transfer, 2) Fracture mechanics, 3) Average stress-average strain laws attributed to tensile concrete and 4) Average stress-average strain laws attributed to reinforcement. Focussing on the latter two smeared approaches and using experimental data collected by the authors, this paper investigates the versatility of the expressions proposed in the current regulations [by simple interpolation between uncracked (I) and fully cracked (II) deformation states of RC] and well-known tension-stiffening

models.

Most of the tension-stiffening models, applying the constitutive equation for concrete (Bazant and Oh (1984), Vecchio and Collins (1986), Hsu (1996), Kaklauskas and Ghaboussi (2001), Gribniak (2009)) or steel (Kaklauskas *et al.* (2011c), Model Code 2010 (2012)) are equivalent. However, among the models there are two sub-types assuming that the tensile behaviour is independent (Vecchio and Collins (1986), Collins *et al.* (1996) and Hsu (1996)) or dependent (Kaklauskas (2001)) on the tensile reinforcement steel ratio. In this study, the following tension-stiffening models are considered:

Vecchio (1986) & Collins (1996)

$$\sigma_c = \frac{f_{ct}}{\sqrt{1 + 500\varepsilon_c}} \quad (1)$$

Hsu (1996)

$$\sigma_c = f_{ct} \cdot \left(\frac{\varepsilon_{cr}}{\varepsilon_c} \right)^{0.4} \quad (2)$$

Kaklauskas (2001)

$$\sigma_c = 0.625 \cdot f_{ct} \left(1 - \frac{\bar{\varepsilon}_c}{\beta} + \frac{1 + 0.6 \cdot \beta}{\beta \cdot \bar{\varepsilon}_c} \right) \quad (3)$$

with $\bar{\varepsilon}_c = \frac{\varepsilon_c}{\varepsilon_{cr}}$, $\varepsilon_{cr} = \frac{f_{ct}}{E_c}$; $\beta = 32.8 - 27.6 \cdot \rho + 7.12 \cdot \rho^2$ ($\rho < 2\%$), $\beta = 5$ ($\rho \geq 2\%$)

The method proposed by EC-2 (2004), also included in MC2010 (2012), is based on the interpolation between States I and II. This interpolation can be applied to stresses, axial forces and bending moments. The formula is,

$$\kappa_m = \kappa_I \cdot (1 - \zeta) + \kappa_{II} \cdot \zeta, \quad \zeta = 1 - \beta_1 \beta_2 \left(\frac{M_{cr}}{M} \right)^a, \quad a = 2 \quad (4)$$

where κ_m is the effective curvature interpolated between the values obtained for State I (non-cracked) κ_I and State II (fully cracked) κ_{II} . The interpolation factor ζ depends on two non-dimensional factors, β_1 and β_2 , both equal to 1 for short-term loads, and the relation between the cracking moment, M_{cr} and the actual moment M .

Walraven (CEB-FIP (2009)) proposes a simplified method based on the formulation of the Model Code 90 (1990), equivalent to that of Model Code 2010 (2012).

The ACI 318 technique (2011) is based on the method proposed by Branson (1963, 1977), which uses the concept of the effective moment of inertia.

$$I_e = \left(\frac{M_{cr}}{M} \right)^a \cdot I_g + \left[1 - \left(\frac{M_{cr}}{M} \right)^a \right] \cdot I_{II}, \quad a = 3 \quad (5)$$

Here I_g is the moment of inertia for uncracked concrete section ignoring reinforcement; I_H is the moment of inertia for the fully cracked section; M is the applied moment at centre span for simply supported beams or at the embedment for cantilevers (slightly more elaborated formulations are applied for undetermined structures) and M_{cr} is the cracking moment.

2.2 Curvature analysis

To obtain a moment-curvature relationship it is necessary to solve a normal stresses problem (Ghali *et al.* (2012)); namely, the equilibrium of a RC cross-section subjected to an axial force and a bending moment. Thus, as established by the continuum mechanics, it is necessary to solve at the same time a set of constitutive, compatibility and equilibrium equations. The resolution of the problem provides the parameters, which define the strain-plane: baricentric strain and curvature.

To solve the sectional problem, the method chosen in this work is the well-known multilayer method (Kaklauskas (2004)), in which the cross section is divided into a series of layers with a reduced thickness whose properties can be easily determined assuming that the fibres are rectangular and that an effective elastic modulus represents the whole behaviour of the fibre.

The compatibility equations used in this paper are the classical adopted in literature for service analysis. The first hypothesis is perfect bond (the “no-slip” condition) between concrete and steel. It implies that the steel and the surrounding concrete have the same strain. The second is the Navier-Bernoulli hypothesis, which from a practical point of view implies that the strain-profile can be represented as a plane.

$$\varepsilon(y) = \varepsilon_0 + \kappa(y - Y_{ref}) \quad (6)$$

Finally, it is necessary to solve the equilibrium equations for axial forces and bending moments, which are obtained equating internal and external forces as follows,

$$\begin{aligned} N &= \int_{A_c} \sigma_c dA_c + \int_{A_s} \sigma_s dA_s = 0 \\ M &= \int_{A_c} \sigma_c y dA_c + \int_{A_s} \sigma_s y dA_s \end{aligned} \quad (7)$$

Combining all the equations (constitutive, compatibility and equilibrium), the following system is obtained:

$$\begin{aligned} EA_h \varepsilon_0 + EB_h \kappa &= 0 \\ EB_h \varepsilon_0 + EI_h \kappa &= M \end{aligned} \quad (8)$$

Eq. (8) provides the parameters, which define the strain-plane: baricentric strain and curvature; and consequently the moment-curvature and the moment-baricentric strain diagrams can be obtained. The parameters EA_h , EB_h and EI_h are the area and the first and the second cross-section moment of inertia respectively, homogenized with respect some material (generally concrete) and multiplied by the elasticity modulus of this material. When the materials behave elastically these coefficients are constant and the system is easily solved. Something similar happens if the classical hypothesis applies because the nonlinear system it is easily solved by a second-degree equation whose unknown is the neutral fibre location in pure bending (Ghali *et al.* (2012)) or a third-degree equation (for a rectangular cross-section) in case of axial force combined with bending (Perez

Caldentey *et al.* (2012)). Once location of the neutral fibre is known, since it is assumed the concrete cannot resist tensile forces, only the concrete under compression must be used to obtain mechanical properties of the cracked concrete cross-section and the system is solved immediately. However, if complex constitutive equations are used to simulate the plastic range of the materials or tension-stiffening effect iterative methods are required to solve Equation (8).

In case of using the classical hypothesis, time-dependent effects can be introduced in Equation (9) in a simple way, using the Trost method (Trost (1967), Bazant (1972)). In this method, the instantaneous elastic modulus of concrete E_{c0} is replaced by an effective modulus E_c which is expressed as $E_c = E_{c0}/(1 + \chi\phi)$, being χ the ageing coefficient (whose value is approximated to 0.80) and ϕ the creep coefficient. Thus, Equation (8) becomes,

$$\begin{aligned} EA_h \varepsilon_0 + EB_h \kappa &= EA_c \varepsilon_{cs} \\ EB_h \varepsilon_0 + EI_h \kappa &= M + EB_c \varepsilon_{cs} \end{aligned} \quad (9)$$

The parameters EA_h , EB_h and EI_h are the same defined before, now using the modulus E_c , adjusted to the time period in which the shrinkage takes place. A group of fictitious internal forces, which represent the imposed deformation effects, must be accounted in order to determine correctly the strain planes (Ghali *et al.* (2012)). The parameters EA_c and EB_c are the area and the first cross-section moment of inertia of the concrete cracked section, respectively, without considering the steel reinforcement contribution. These parameters are multiplied by the free shrinkage strain ε_{cs} to obtain the corresponding fictitious axial force and bending moment to be added to external forces.

2.3 Inverse (constitutive modelling) technique

Unlike the deformation (direct) analysis, which is used for prediction of structural response using a specified constitutive model, the inverse analysis aims at determining parameters of the model based on the response of the structure. Kaklauskas and Ghaboussi (2001) have formulated the principles of the inverse technique for deriving tension-stiffening relationships using test data of RC flexural members. For a given moment-curvature diagram, an average stress-average strain tension-stiffening relationship was computed from the equilibrium equations of axial forces and bending moments using the layer section model (Kaklauskas (2004)). The layer section model was employed for computation of the internal forces. The inverse analysis was performed with incrementally increasing bending moment. The equilibrium equations (8) were solved for each loading stage yielding a solution for the coordinate of the neutral axis and the concrete stress in the extreme tension fibre. Since the extreme fibre had the maximum strain, other tension fibres of concrete had smaller strains falling within the portion of the already determined stress-strain diagram. The derived model enables to simulate the same moment-curvature response as was obtained in the tests. The inverse analysis is based on the following approaches and assumptions:

- Average strain, also called as smeared crack, approach.
- Linear strain distribution within the depth of the section implying perfect bond between layers.
- All concrete layers in the tension zone follow a uniform stress-strain law.

The latter assumption of a uniform stress-strain tension-stiffening law for different layers allows reducing the dimension of the solution to a single non-linear equation. The following experimental data of flexural RC members can be used for the inverse technique:

- Bending moment vs. average strain of the extreme fibre of compressive concrete;
- Bending moment vs. average strain of the extreme fibre of tensile concrete;
- Bending moment vs. average strain of the tensile reinforcement;
- Bending moment vs. mid-span deflection;
- Bending moment vs. curvature;
- Average stress vs. average strain of tensile reinforcement.

Recent investigations (Kaklauskas *et al.* (2011b)) have demonstrated that the inverse technique may serve as a powerful tool for constitutive analysis of flexural RC members. It may be relatively easy extended to other tension-stiffening approaches, such as steel-related or stress transfer models. The current study deals with the inverse technique modified by Gribniak (2009) and Kaklauskas and Gribniak (2011a), and applies two most effective inverse techniques

1) A steel-related modelling (Kaklauskas *et al.* (2011c)) is used for analysis of the tension-stiffening stresses induced in the section by varying arrangement of rebars;

2) A concrete-related modelling algorithm (Kaklauskas *et al.* (2009)) is used for the “elimination” of the shrinkage effect from the test data (Kaklauskas and Gribniak (2011a)).

2.4 Assessing the effect of shrinkage

It is known that, even at first loading, free shrinkage of concrete may well exceed the cracking strain. The shrinkage strain, restrained by reinforcement, significantly affects the cracking resistance and short-term deformations of RC members. Kaklauskas and Gribniak (2011a) have developed a numerical procedure for the “elimination” of the effect of shrinkage from experimental moment-curvature and tension-stiffening diagrams. In this manuscript, these modified relationships are referred to as “free-of-shrinkage”. The shrinkage elimination procedure is performed in the following steps sketched in Fig. 1.

Step 1. Using the moment-curvature diagram (Fig. 1a), the stress-strain relationship is derived (Fig. 1b) by the inverse technique.

Step 2. Using the derived stress-strain (tension-stiffening) relationship, the moment-curvature diagram is calculated by the technique described in Section 2.2. In order to eliminate the effect of shrinkage, the shrinkage strain of concrete is taken positive, i.e. as the expansion strain. The

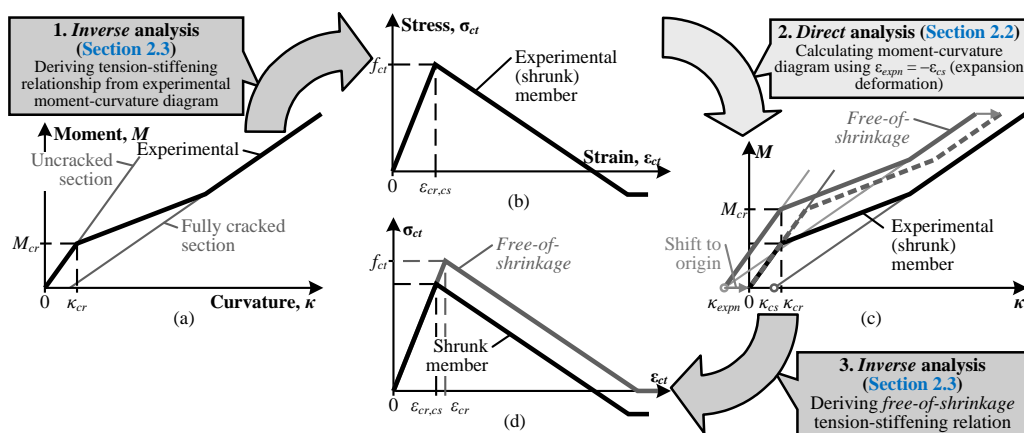


Fig. 1 Deriving “free-of-shrinkage” moment-curvature and tension-stiffening relationships

Table 1 Geometrical properties of test specimens.

Cross-section	12-20-00/10/30	12-70-00/10/30	25-20-00/10/30	25-70-00/10/30
b [m]	0.35	0.35	0.35	0.35
h [m]	0.45	0.45	0.45	0.45
d [m]	0.412	0.362	0.4055	0.3555
c [m]	0.038	0.088	0.0445	0.0945
\varnothing (A_{s1}) [mm]	12	12	25	25
\varnothing (A_{s2}) [mm]	12	12	12	12
A_{s1} [cm ²]	4.52	4.52	19.63	19.63
A_{s2} [cm ²]	2.26	2.26	2.26	2.26
$\rho=A_{s1}/bd$	0.31%	0.36%	1.36%	1.55%

calculated free-of-shrinkage moment-curvature diagrams are shown in Fig. 1c along with the initially assumed curve. It should be noted that due to the expansion of concrete, an initial negative curvature was obtained. In absolute value, it is equal to the initial curvature (the positive one) due to shrinkage.

Step 3. Since an unloaded non-shrunk beam has no curvature, the obtained free-of-shrinkage moment-curvature diagram is shifted to the zero point (dashed line in Fig. 1c). Using this diagram, the free-of-shrinkage stress-strain relationship is obtained by the inverse analysis. This relationship is shown in Fig. 1d along the one obtained from the “test” of shrunk member.

In the present study, this shrinkage elimination method is applied to correct the experimental data using the information provided in Table 1 resulting in “free-of-shrinkage” moment-curvature diagrams. In cases when some material parameters were missed, the respective values are calculated by equations from the Model Code 2010 (CEB-FIP (2012a, 2012b)).

3. Experimental program

Experimental data used in this paper has been obtained in a test program carried out in the Structures Laboratory of the Polytechnic University of Madrid by Perez Caldentey *et al.* (2013) during the year 2009. In this program, 12 beams were tested. The beams were designed to study the influence of the following parameters on tension-stiffening:

- \varnothing/ρ_{eff} : half of the beams were reinforced with 4 \varnothing 25 and the other half with 4 \varnothing 12.
- cover: half of the beams had a cover of 20 mm and the other half had 70 mm.
- influence of stirrup spacing: four beams had no stirrups, four had stirrups spaced at 30 cm and the remaining four specimens had stirrups spaced at 10 cm.

The test configuration is presented in Fig. 2 and corresponds to the well-known “four points test”. Hydraulic jacks located at the end of the cantilever spans load a simply supported beam, with a load cell in each support. All beams have a central span of 3.42 m and two cantilever spans of 0.90 m. The jacks apply the load at 0.75 m from each support. Thus, due the fact load is applied only at the ends, and dead weight has a small effect, the central span is subjected to a constant bending moment that allows studying the mean (smeared) behaviour of the beam.

In the central span zone at each side of the beams, there are three lines of digital extensometer

bases (20 cm base) to measure longitudinal surface strains of concrete. One line is located at the side of the beam in correspondence with the location of the compressive longitudinal reinforcement; a second is located at the side of the beam in correspondence with the location of the tensile reinforcement and a third line is located on the top tension face in the same vertical plane as the tensile reinforcement. Four inclinometers were located over the supports (two) and at the external surface of the cantilever face (the other two). Deflections were registered in five points, below the jacks at quarter and mid-span.

Table 2 Concrete properties

Property	Value
concrete type	HA-25/B/20/IIa
cement type	CEM II/AM-VL 42.5R
Probe	cylindrical, Ø15cm
water/cement ratio	0.55
kg cement/m ³	330
additive	plasticizer
Abram's cone [cm]	7.0
density kg/m ³	2280
$f_{cm,7d}$ [MPa]	21.9
$f_{cm,28d}$ [MPa]	26.9

Table 3 Mechanical properties obtained experimentally

Cross-section	12-20-00/10/30	12-70-00/10/30	25-20-00/10/30	25-70-00/10/30
$f_{cm,28d}$ [MPa]	26.9	26.9	26.9	26.9
without shear reinforcement (XX-YY-00)				
Age [days]	56	91	42	84
T [°C]	19.9	22.2	18.8	21.6
RH [%]	38.2	38.2	38.1	38.4
M_{cr}^* [kNm]	29.2	29.4	15.9	29.7
shear reinforcement: 1 stirrup Ø12 each 30 cm (XX-YY-30)				
Age [days]	63	176	110	120
T [°C]	20.3	25.6	23.4	23.9
RH [%]	38.6	34.2	37.0	36.0
M_{cr}^* [kNm]	29.9	30.3	37.2	29.8
shear reinforcement: 1 stirrup Ø12 each 10 cm (XX-YY-10)				
Age [days]	98	190	112	126
T [°C]	22.6	25.5	23.6	24.2
RH [%]	37.8	34.7	36.7	35.5
M_{cr}^* [kNm]	29.5	32.3	29.8	26.6
reference lines (State II)				
Mean Age [days]	72	152	88	110

*deduced from the tests

Table 4 Mechanical properties estimated from the model code 2010 (CEB-FIP (2012a 2012b)).

Cross-section	12-20-00/10/30	12-70-00/10/30	25-20-00/10/30	25-70-00/10/30
without shear reinforcement (XX-YY-00)				
f_{cm} [MPa]	28.5	29.4	27.9	29.3
f_{ct} [MPa]	2.3	2.3	2.2	2.3
E_c [MPa]	30790	31263	30455	31192
Shrinkage, ϵ_{cs} [$\mu\epsilon$]	-440	-514	-398	-502
Creep coeff. ϕ	2.40	2.75	2.21	2.69
Aging coeff. χ	0.87	0.86	0.88	0.86
M_{cr} [kNm]	28.4	28.5	32.2	30.9
$EB_c\epsilon_{cs}$ [kNm]	1.1	0.9	7.7	6.3
shear reinforcement: 1 stirrup $\varnothing 12$ each 30 cm (XX-YY-30)				
f_{cm} [MPa]	28.8	30.3	29.7	29.8
f_{ct} [MPa]	2.3	2.4	2.4	2.4
E_c [MPa]	30915	31754	31420	31488
Shrinkage, ϵ_{cs} [$\mu\epsilon$]	-457	-629	-546	-562
Creep coeff. ϕ	2.48	3.36	2.92	3.01
Aging coeff. χ	0.87	0.84	0.85	0.85
M_{cr} [kNm]	28.6	29.4	34.0	31.4
$EB_c\epsilon_{cs}$ [kNm]	1.1	1.0	9.0	6.5
shear reinforcement: 1 stirrup $\varnothing 12$ each 10 cm (XX-YY-10)				
f_{cm} [MPa]	29.5	30.4	29.7	29.9
f_{ct} [MPa]	2.3	2.4	2.4	2.4
E_c [MPa]	31326	31801	31434	31524
Shrinkage, ϵ_{cs} [$\mu\epsilon$]	-527	-642	-550	-571
Creep coeff. ϕ	2.82	3.40	2.94	3.06
Aging coeff. χ	0.86	0.84	0.85	0.85
M_{cr} [kNm]	29.4	29.5	34.0	31.5
$EB_c\epsilon_{cs}$ [kNm]	1.3	1.0	9.0	6.6
reference lines (state II)				
E_c [MPa]	31053	31659	31234	31420

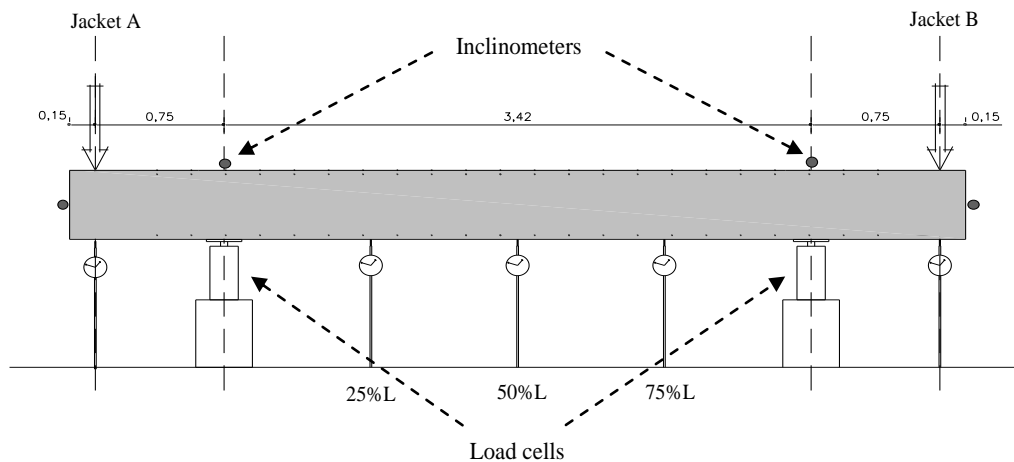


Fig. 2 Test configuration

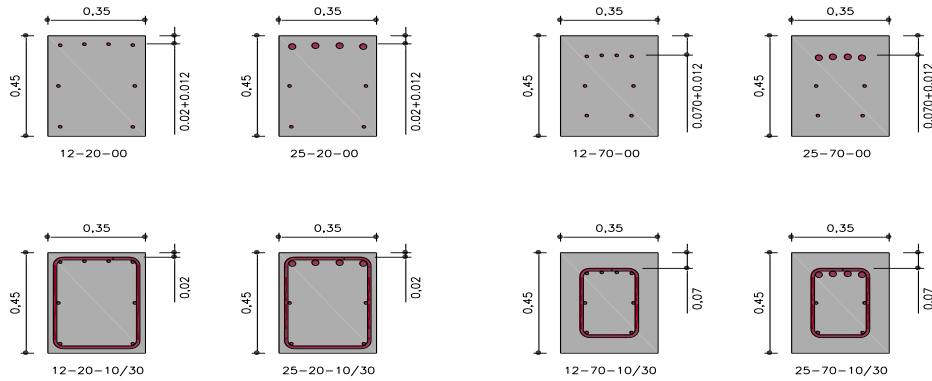


Fig. 3 Test specimen cross-sections

4. Experimental results

Strains measured along the reinforcement fibres are useful to obtain the baricentric strains and curvatures. On the other hand, measures of rotations and deflections can be used to obtain a second estimate of the curvatures and allow a comparison with the strains measured in the reinforcement fibres, thereby testing the quality of the measured data.

In the central span of the specimens of Table 1, there are 17 extensometric bases of 20 cm. Thus, the curvature, κ , can be obtained for each station i and, consequently, the mean value can be determined. In the same way, the rotation variation between the supports is related with this curvature as expressed in Mohr's first theorem.

Also assuming a linear variation of curvatures in the cantilevers, a relation between the rotation in the outer faces and the supports can be obtained:

$$\Delta\theta_{cant,AB} = \int_0^{L_v} \kappa(x) dx = \int_0^{L_v} \frac{1}{2} \kappa_m dx + \int_0^L \kappa_m dx + \int_0^{L_v} \frac{1}{2} \kappa_m dx = \kappa_m (L + L_v) \quad (10)$$

Finally, the half-span deflection can be obtained by a double integration of curvatures,

$$f_{50\%L} = \theta_A \frac{L}{2} + \int_0^{L/2} \int_0^{L/2} \kappa(x) dx dx = \theta_A \frac{L}{2} + \kappa_m \frac{L^2}{2}, \quad \theta_A = \frac{1}{2} \Delta\theta_{AB} = \frac{1}{2} \kappa_m L \quad (11)$$

In Equation (11), it is necessary to know the value of the rotation over the supports, which can be obtained from the measures carried out with inclinometers or from the curvatures, using the Mohr's first theorem.

The use of different sensors allows the detection of inaccuracies during the test by simple comparison between measurements. Fig. 4 shows the correlation between the rotations measured by inclinometers and the rotations obtained by integration of curvatures (left) and the correlation between the deflections at mid-span measured by linear variable differential transformers, LVDT, and the deflections obtained by double integration of curvatures (right). It can be seen that deflections obtained from the measured curvatures are slightly larger than those measured with LVDT.

Fig. 5 shows a summary of experimental results obtained for all specimens from the main

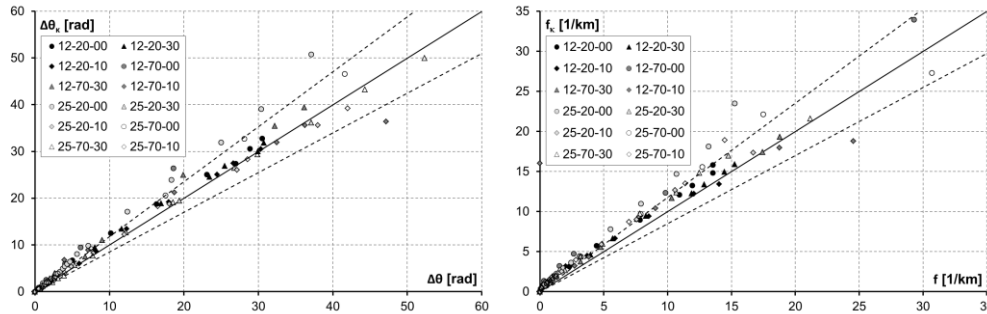


Fig. 4 Left: Experimental rotations (abscissa) vs. rotations obtained from integration of curvatures (ordinate). Right: Experimental deflections (abscissa) vs. deflections obtained from double integration of curvatures (ordinate)

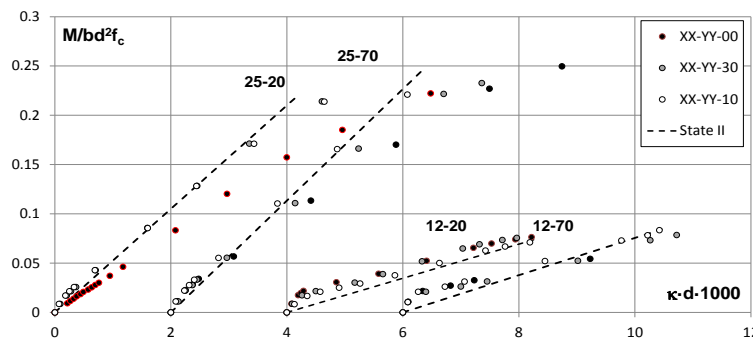


Fig. 5 Normalized experimental $M-\kappa$ relationships obtained from surface strains of concrete

experimental program (Section 3.1) in form of moment-curvature relationships ($M-\kappa$). For each subgroup, a reference line that represents the theoretical behaviour in state II for a concrete with a given mean age (see parameters in Tables 3 and 4) is plotted. It is important to note that the analytical values presented in these graphs imply the use of classical constitutive equations for serviceability as explained in Section 2.2. Thus, the reference line does not reproduce any non-linearity due to crushing of compressive concrete or yielding of steel. Simply, this curve is extended until the maximum value measured experimentally is reached.

5. Discussion of results

5.1 Experimental data modified by inverse method (“free-of-shrinkage” diagrams)

As commented previously, even for short-term tests, experimental results obtained from surface strains of concrete are affected by rheological strains. Thus, in order to remove these effects and obtain a reliable result, the measurements must be modified using the inverse methodology described in Sections 2.3 and 2.4. Fig. 6 is the same results as in Fig. 5, but now eliminating the shrinkage effect.

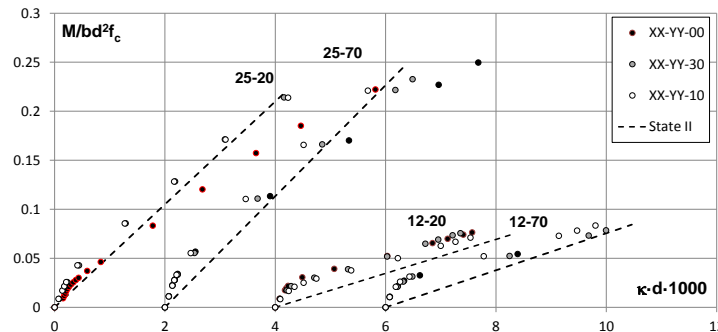


Fig. 6 Normalized M - κ relationships. Experimental values corrected by inverse methodology

Simple observation of curves presented in Fig. 6 allows identifying a horizontal displacement (a reduction) of the values corrected by the inverse technique. This curvature difference is almost constant independently of bending moment. For a cross section with tensile reinforcement subjected only to a shrinkage deformation, due to perfect bond between concrete and steel, as a simplification it can be assumed that there is no increment of concrete strain at the steel fibre whereas the imposed strain develops freely in the compressive concrete fibre. The real situation is not far from this simplification (Ezeberry Parrotta (2011)). Thus, this curvature difference can be estimated approximately as the ratio between the free shrinkage and the effective depth of tensile reinforcement.

As the age at which the test is carried out increases, the shrinkage effect is more pronounced. In some cases, this effect, referred to as “negative tension-stiffening”, can produce a reduction of the specimen stiffness well below the “fully cracked” behaviour. On the other hand, in case of values corrected by the inverse method (“free-of-shrinkage” data), this reduction is not observed. However, an additional reduction can occur for large values of bending moment for which the materials yield and the classical hypothesis presented in Section 2.2 are no longer valid. It must be said that, for Beam 25-20-00, which was accidentally cracked before the loading, it is verified an altered behaviour due to its own load history.

For beams 25-20 and 25-70, there are still some “corrected” experimental points outside the zone delimited by reference lines. However, in this case, this is due to nonlinear material behaviour of materials (concrete crushing and/or steel yielding) which have not been included in the simplified constitutive equations adopted for the reference lines. The results obtained confirm the importance of a correct assessment of the shrinkage effect in the deformation analysis of RC beams in flexure.

5.2 Moment-curvature relationship

This section is dedicated to analyse the adequacy of the tension-stiffening models summarized in Section 2.1. Figs. 7 and 8 present an analytical-experimental comparison using the moment-curvature diagram for beams 12-20/70-10 and 25-20/70-10, respectively. To clarify the presentation analytical results are given in groups of three. In all graphs, there are two reference lines, which represent states I and II, and two set of experimental results: the pure experimental data obtained from longitudinal surface strains of concrete and the “free-of-shrinkage” values

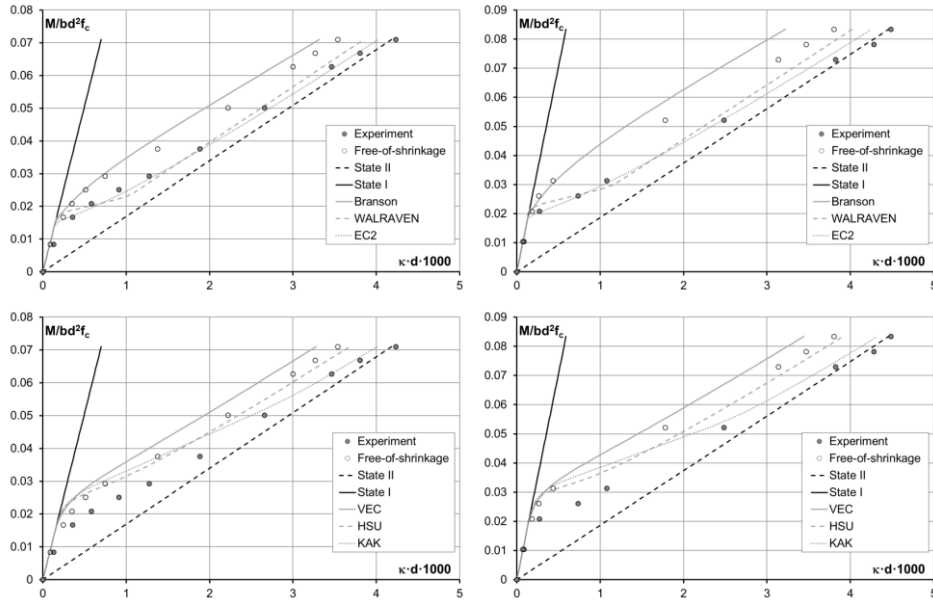


Fig. 7 Normalized $M-\kappa$ diagrams: comparison for beams 12-20-10 (left) and 12-70-10 (right)

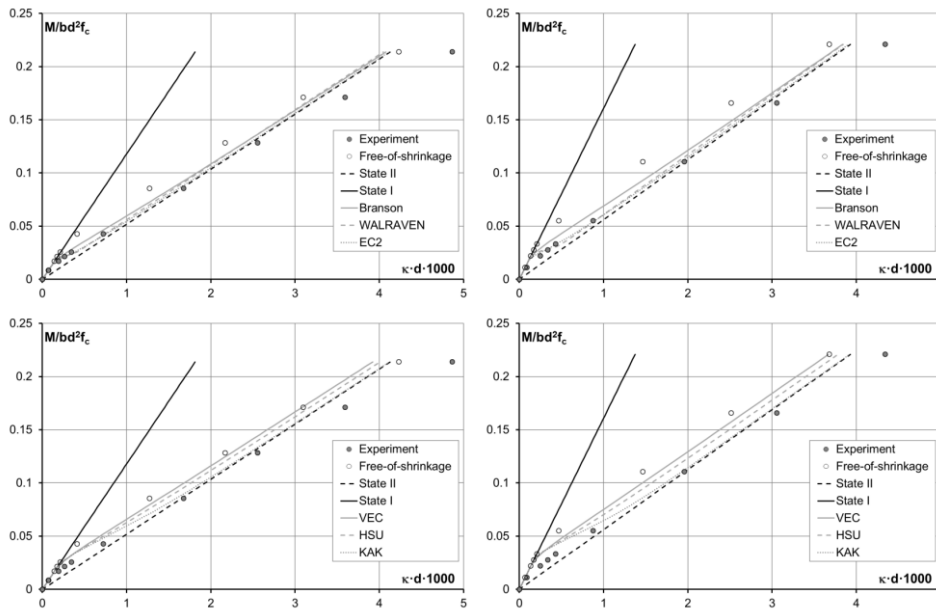


Fig. 8 Normalized $M-\kappa$ diagrams: comparison for beams 25-20-10 (left) and 25-70-10 (right)

obtained by the inverse method (Section 2.3). The upper plot present the results obtained using the interpolation methods proposed by Branson (1963), EC-2 (2004) and Walraven (CEB-FIP (2009)). The lower plot present results obtained for models which modify the tensile constitutive equation for concrete: Vecchio and Collins (1986), Collins *et al.* (1996), Hsu (1996) and Kaklauskas (2001).

5.3 Tension-stiffening laws for materials

In a numerical modeling, shrinkage can be taken into account in two ways: directly or indirectly. In the first case, it can be assessed as a prescribed deformation or a fictitious force. This analysis should be based on material (tension-stiffening) models with the excluded shrinkage effect. Such models can be obtained from experimental data with eliminated shrinkage. These are hereafter called the free-of-shrinkage relationships. Until nowadays, only a few such models were proposed. In this respect, the studies conducted by Gilbert (2001) and Bischoff (2001) should be mentioned. In the second case, more general and common for engineering practice, analysis is performed using the laws where tension-stiffening is coupled with shrinkage.

The inverse method allows the determination of the tension-stiffening laws which match the experimental results. These laws can be obtained for either concrete or steel. The selection of the material in which the law is applied is arbitrary, both laws are equivalent and produce the same results.

Thus, Figs. 9 and 10 show the laws obtained for concrete and steel, respectively. Again, the results are presented in four groups. In order to make a comparison, only the analytical law proposed by Vecchio (1986) and Collins (1996) is used for concrete and the law recommended by the Model Code 2010 (2012) is used for steel.

Fig. 9 shows that analytical results obtained for 12 mm rebars are closer to experimental data than the results obtained for 25 mm rebars. On the other hand, the comparison between analytical and experimental values is better for concrete cover of 20 mm than 70 mm. The beam 25-20-00, cracked before the test, shows a strong reduction in the tension-stiffening law.

It is well known that tension-stiffening effect is relatively low (at the same strain level) in RC elements with increased area of tensile reinforcement – due to increased stiffness of the section, the particular strain is reached at the reduced tension-stiffening stress value. Thus, due to above effect and accumulative nature of the computation errors (Gribniak *et al.* (2012)), the inverse procedure is extremely sensitive for increment in reinforcement ratio that may produce distortion of the derived concrete-related tension-stiffening laws.

Fig. 10 shows tension-stiffening laws related to steel. The derived curves can be used for a comparative analysis of the tension-stiffening effects assessed for the same level of stress in reinforcement. They might be also effective for assessing reduction of stiffness of the cracked section with increased deformations of rebars. Fig. 10 evidences that tension-stiffening plays a prominent role assessing deformations of lightly reinforced elements (having $\varnothing 12$ mm bars).

Comparison of the laws recommended by Model Code and diagrams derived from the test data with eliminated shrinkage effect shows a significant underestimation of tension-stiffening by the MC2010 (2012). This reflects the need to improve the Model Code formulation in order to adequately assess shrinkage effects.

It was shown by Kaklauskas and Gribniak (2011a) that, seeking adequacy of serviceability analysis results, numerical (finite element) modelling of RC elements should include the shrinkage effect separated from the material models. Such separation might be done applying prescribed shrinkage deformations contemporarily with the free-of-shrinkage material (tension-stiffening) laws. However, common design code models, empirically deduced from the experimental data of (shrunk) RC elements, include the shrinkage effect in integral manner and, sometimes, cannot be used for the adequate modelling of RC. Therefore, separation of shrinkage from code equations becomes of vital importance. The following study deals with the deformation models specified by two of the main regulations: EC-2 (or the Model Code 2010) and ACI-318 (Branson).

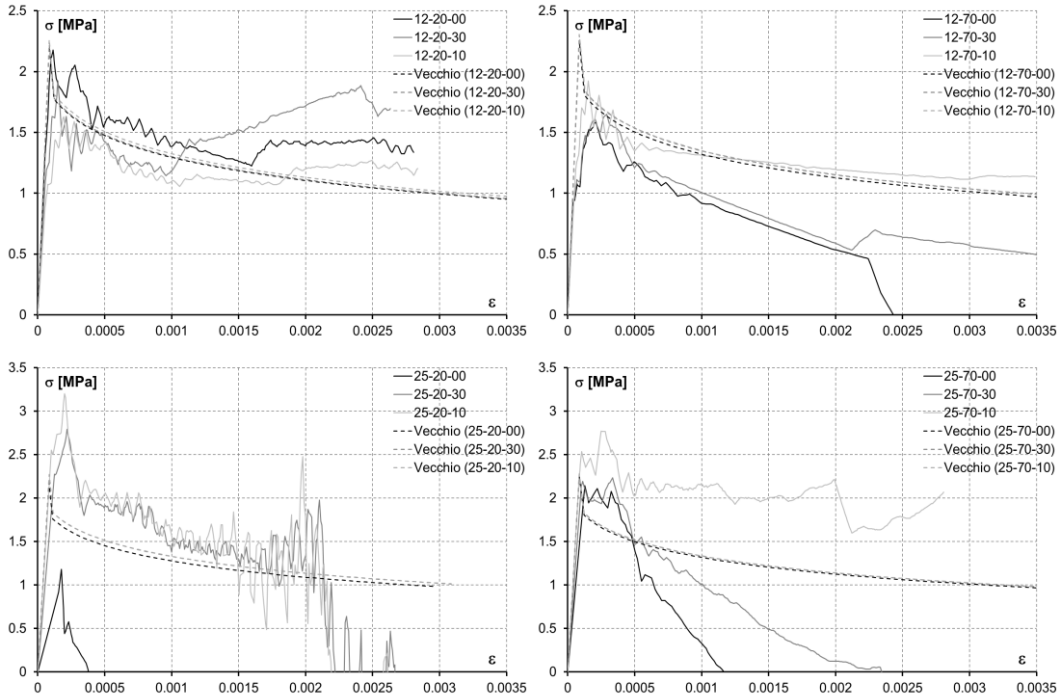


Fig. 9 Inversely obtained average stress-average strain (tension-stiffening) relationships of concrete

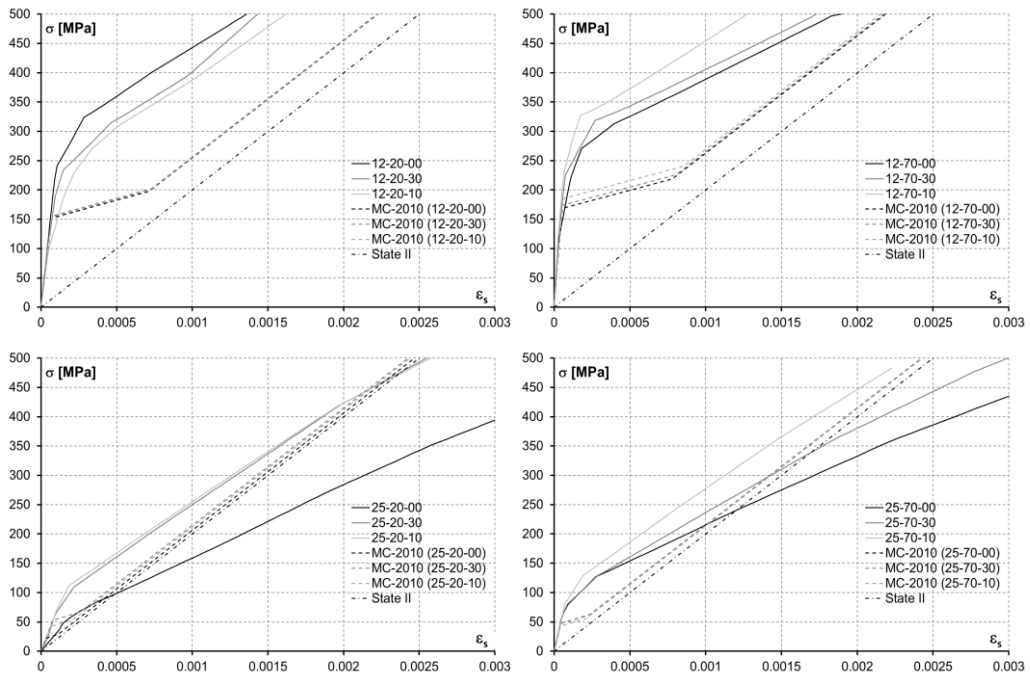


Fig. 10 Inversely derived stress-strain (tension-stiffening) relationships of steel

6. Interpolating deformations between uncracked (I) and cracked (II) states

It was shown by Gribniak *et al.* (2013b) that, in the cases of high demands on accuracy, shrinkage should be taken into account in the numerical analysis (what is not a common practice). Using free-of-shrinkage moment-curvature diagrams, the interpolation factor ζ (as specified by EC-2) can be assessed from Equation (4)

$$\zeta = \frac{\kappa_m - \kappa_I}{\kappa_{II} - \kappa_I} \quad (12)$$

κ_m being the free-of-shrinkage curvature obtained from the experimental data by the inverse method and κ_I and κ_{II} analytical curvatures obtained for States I and II, respectively. It is interesting to keep the mathematical expression presented in Equation 5 and adjust the power a in order to match the experimental results. Thus, these values are obtained by using least squares approach and experimental data corresponding to greater bending moments measured within the serviceability range.

In case of Branson method, the mean curvatures are obtained by dividing the bending moments by the effective modulus of inertia and introduced in Equation (5), together with the values obtained for States I and II, to obtain the corresponding value of ζ to be used in the following comparisons.

The first comparison is presented in Fig. 11, where the estimations of ζ using Equation (12) and the pure experimental data are presented and compared with EC-2 (Equation 4, $a = 2$) and ACI (Branson, Equation 5, $a = 3$) estimations. In this case, the values of the optimised values of parameter a were difficult to obtain using least squares. In section 5.1 was pointed out that at the cracking moment there is a sudden release of compression stresses, produced by the previous shrinkage, at the longitudinal reinforcement which induces an increase of curvature. Thus, a lot of results fall away of the zone defined by States I and II avoiding the use of Equation (4) to obtain the parameter a .

The comparison between the EC-2 results and the Branson approach allow confirm a well-known aspect of Branson formulation: for lower steel ratios and relations M/M_{cr} closer to one, Branson approach tends to give a lower curvature compared with EC-2. Thus, estimations of deflection based on Branson approach are on the unsafe side in this zone. Experimental results obtained for 12-20 specimens confirm this fact; however, this conclusion is not so clear in 12-70 results. In any case, for elements with lower steel ratios as slabs, deflections should be calculated using EC-2 formulation. As the bending moment increase, the difference between both approaches reduces strongly. In the same way, for higher steel ratios practically there is not an important difference. In both cases, the reason is in the reduction of tension-stiffening effect as the bending moment and steel ratio increase.

In Fig. 12, which has the same shape as Fig. 11, the “free-of-shrinkage” experimental measures are presented. Estimations according EC-2 ($a = 2$) and Branson ($a = 3$) are included together with a new curve which represents the best estimation of the exponential parameter a .

In each graph the best estimation of the parameter a , adjusted by least squares, is indicated above each family of experimental data. For beams 12-20-00/10/30, $a = 0.98$; for beams 25-20-00/10/30, $a = 0.94$; for beams 12-70-00/10/30, $a = 1.71$ and for beams 25-70-00/10/30, $a = 1.41$. As can be seen, this figure shows clearly how the expression proposed by the EC-2 ($a = 2$) overestimates the value of ζ for this particular set of data.

Due the reduced number of experiments analysed, the same analysis is repeated for the

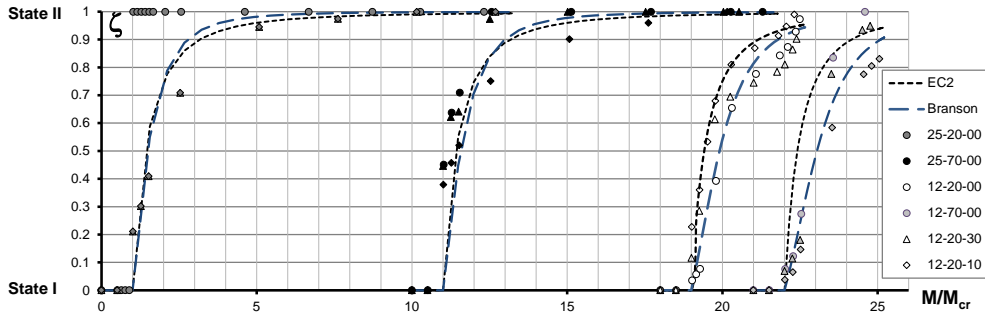


Fig. 11 Variation of the interpolation coefficient ζ with loading. Pure experimental data

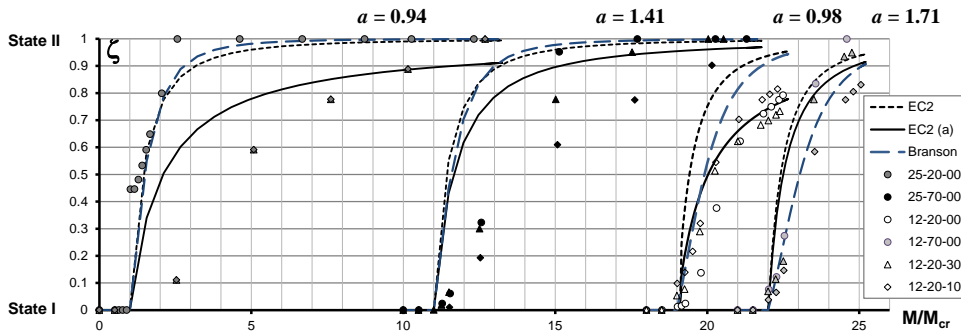


Fig. 12 Variation of the interpolation coefficient ζ with loading. Free-of-shrinkage results

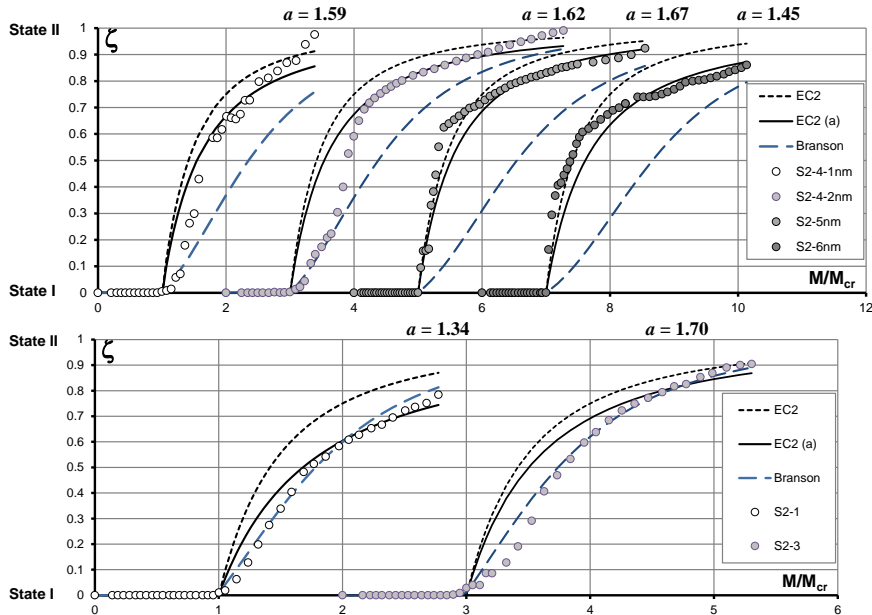


Fig. 13 Variation of the interpolation coefficient ζ with loading (test data reported by Gribniak)

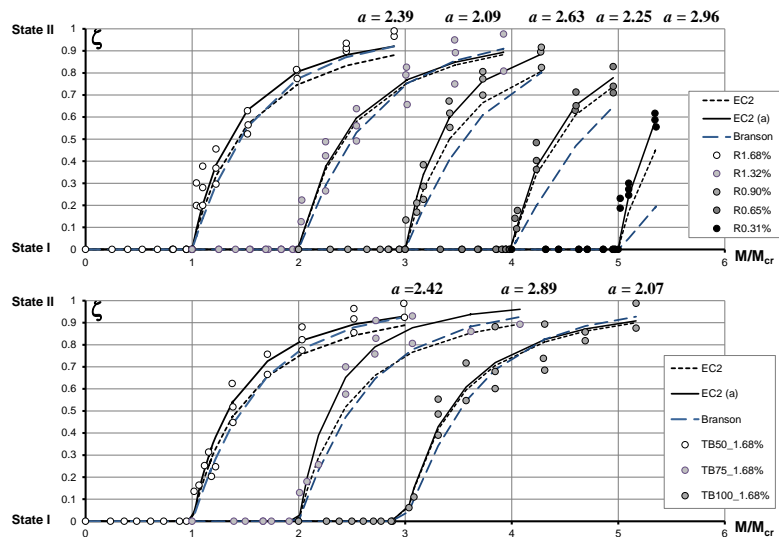


Fig. 14 Variation of the interpolation coefficient ζ with loading (test data reported by Bach and Graf)

experimental data described in the Annex. Fig. 13 shows the results obtained from the experimental data provided by Gribniak *et al.* (2013a) that are corrected by the inverse methodology (Section 2.4). In this case, all the specimens have the same reinforcement ratio and the difference can be found in the type of reinforcement used (GFRP or steel rebars). In general, it can be seen that EC-2 gives a better approach for beams reinforced with GFRP bars, whereas, for steel reinforced beams, Branson's model is more accurate.

Fig. 14 gives the results obtained for the tests made by Bach and Graf (1917), whose main characteristics are detailed in Table 5, see the Annex. In all cases, the power a was obtained greater than two. As the reinforcement ratio increases Branson and the EC-2 tends to give the same results. On the other hand, for R-beams, as the reinforcement is reduced the Branson approach tends to give less accurate results compared with the EC-2. It is important to note that the data reported by Batch and Graf are not compensated by the shrinkage records resulting in the increased power a in respect to other tests.

7. A proposal for improvement of the actual EC-2 formulation

From the analysis carried out at previous section, it can be stated that shrinkage effects can be eliminated (or separated) from the deflection prediction model of EC-2 by reducing the value of the parameter a . However, as showed by the experimental results, shrinkage occurring since the concrete casting until the moment in which the loads are applied must be accounted to obtain a realistic estimation of the deflections. Thus, in this section a new way of estimate the deflection is studied. This method requires the sum of two parts: the first one referring to instantaneous behaviour and the second one that quantifies the rheological history of the member until the moment in which the external short-term loads are applied.

In order to find a simplified factor to represent the short-term behaviour, to be used in place of

the actual value $a = 2$, the results obtained in previous section are analysed. In section 5.3 were found some discrepancies for tension-stiffening laws obtained for 70 mm concrete cover. Thus, to investigate the probable influence of concrete cover, the sensibility of the results obtained to parameter d/h is plotted in Fig. 15. In this figure, the relationship between the parameter a and the relation d/h for all beams in which the shrinkage effect was removed, is presented. For beams with 20 mm ($d/h = 0.92$) concrete cover, excepting the special case of specimen 25-20-00, the value of the parameter is close to 1.00 with little scatter, whereas for 70 mm ($d/h=0.80$) the mean value is about 1.50, showing an important scattering. Although, if in this last case a is evaluated using only the results from 12-70-10 and 25-70-10, the value of a can be considered closer to 1.00 (0.87-1.22). These results states that for short-term estimations of deflections and for high relations of the parameter d/h (above 0.90) the exponential value could be reduced from 2 to a value near to 1. However, for relations above 0.90, the scatter detected avoids a similar conclusion.

Fig. 16 present the comparison between the coefficient ζ , obtained from the measured deflections and the estimations obtained using Equation (4) for the mean values of a obtained in previous section ($a = 1$ for 20 mm concrete cover and $a = 1.5$ for 70 mm concrete cover, adding $a = 2$ as recommended by EC-2).

As commented previously, the reduction of the parameter a should be accompanied of an additional term related to shrinkage effect. This separation of effects can improve the estimation, making it more general to account different rheological situations. In order to quantify the increase of curvature due to the negative tension-stiffening effect, the difference between the total deflection measured and the deflection obtained from “free-of-shrinkage” curvatures Δf is analysed.

Fig. 17 represent the relation between this increase of deflection measured and the deflection f_{cs} produced by a simplified mean curvature κ_{cs}^* that is obtained as the ratio between the free shrinkage strain and the effective depth of reinforcement, $\kappa_{cs}^* = \varepsilon_{cs}/d$. This curvature represents a simplified value produced by the rotation of the section around the tensile reinforcement (full internal constraint to imposed deformation) and the free shrinkage of the upper concrete fibre. In the same figure, two horizontal reference curves, which express the difference between the deflections obtained in State II and I, are plotted. The numerical values are obtained using the hypothesis presented in section 2 (methodology) and the parameters presented in tables 1 to 3, solving the Equation (9). The nature of the experimental campaign makes the elastic curvatures induced by shrinkage invisible in the measures carried out, so this curvature must be subtracted in numerical estimations in order to make the comparison. It is evident that at the time of calculate the deflection in real structures the elastic contribution must be taken into consideration.

As can be seen in Fig. 17, for specimens 12-20 and 12-70 the relations obtained are between 0.40 and 1.20. Although some points exceed the theoretical value, 0.91 for 12-20 and 1.05 for 12-70, which should represent an upper limit, the results are acceptable due the uncertainties involved in the analysis. On the other hand, for specimens 25-20 and 25-70 the relations obtained are between 0.30 and 0.70. In this case the analytical reference curves, 0.53 for 25-20 and 0.72 for 25-70, are exceeded only for relation M/M_{cr} greater than 10. The reduction observed in the upper limit of these last specimens ($\varnothing 25$ rebars) reveals the influence of the tensile reinforcement, which restrains an important part of the free shrinkage.

Thus, a safe estimation of the deflection can be made calculating first the deflections produced by short-term loads using a reduced value of a , and adding the shrinkage deflection, using the classical hypothesis in State II. In Fig. 18 analytical estimations (f_{est}) using $a = 1.00$ for relation $d/h = 0.92$ (concrete cover 20 mm) and $a = 1.50$ for relation $d/h = 0.80$ (concrete cover 70 mm) are

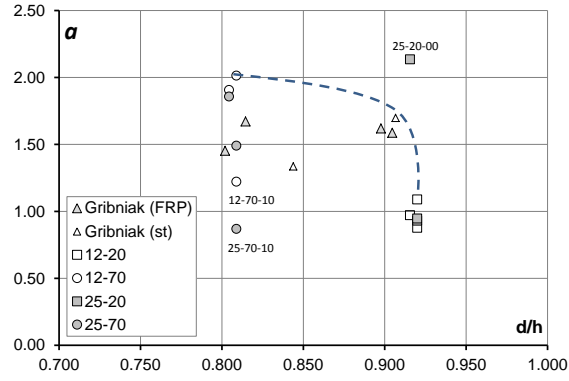


Fig. 15 Variation of a parameter with d/h ratio

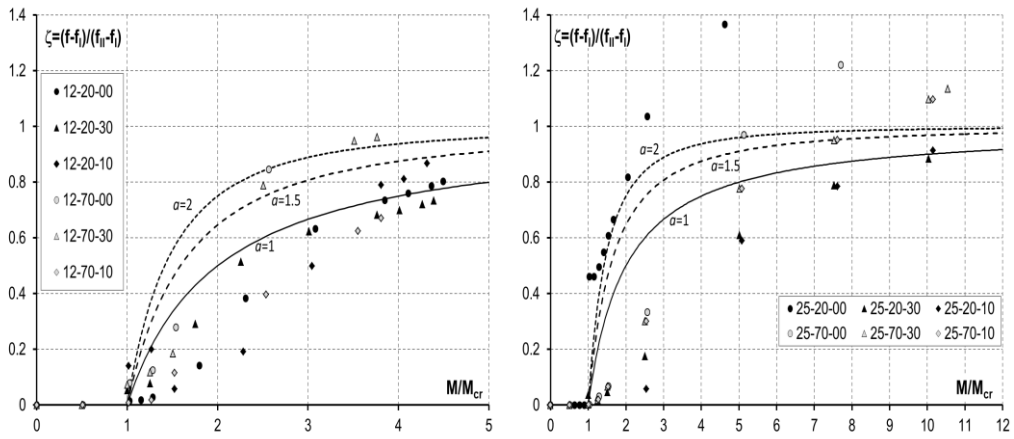


Fig. 16 Value of the interpolation coefficient ζ deduced from deflections

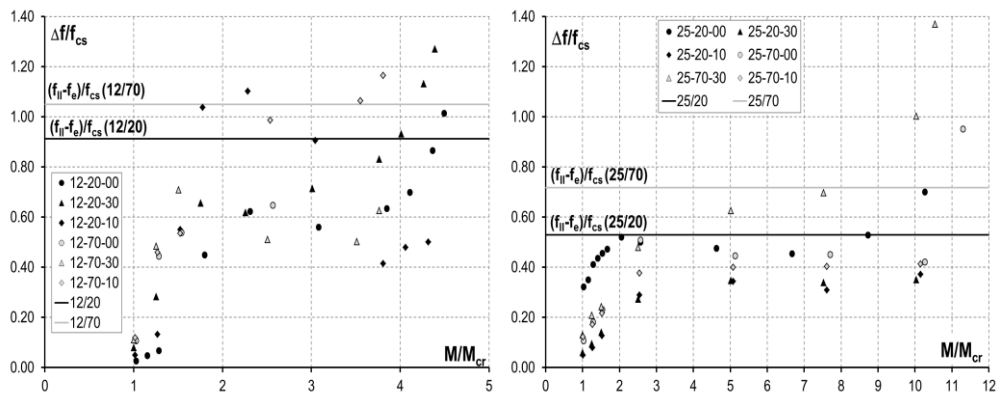


Fig. 17 Additional deflection produced by shrinkage effects

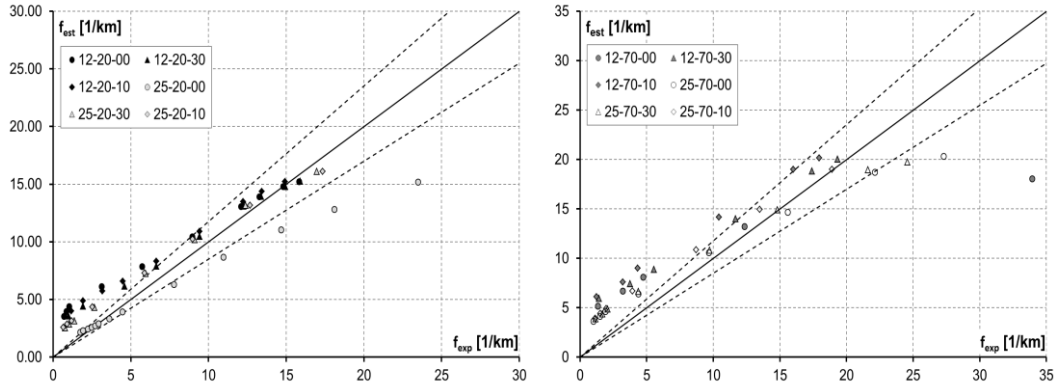


Fig. 18 Calculated vs. measured deflections. Left: $a = 1.00$. Right: $a = 1.50$

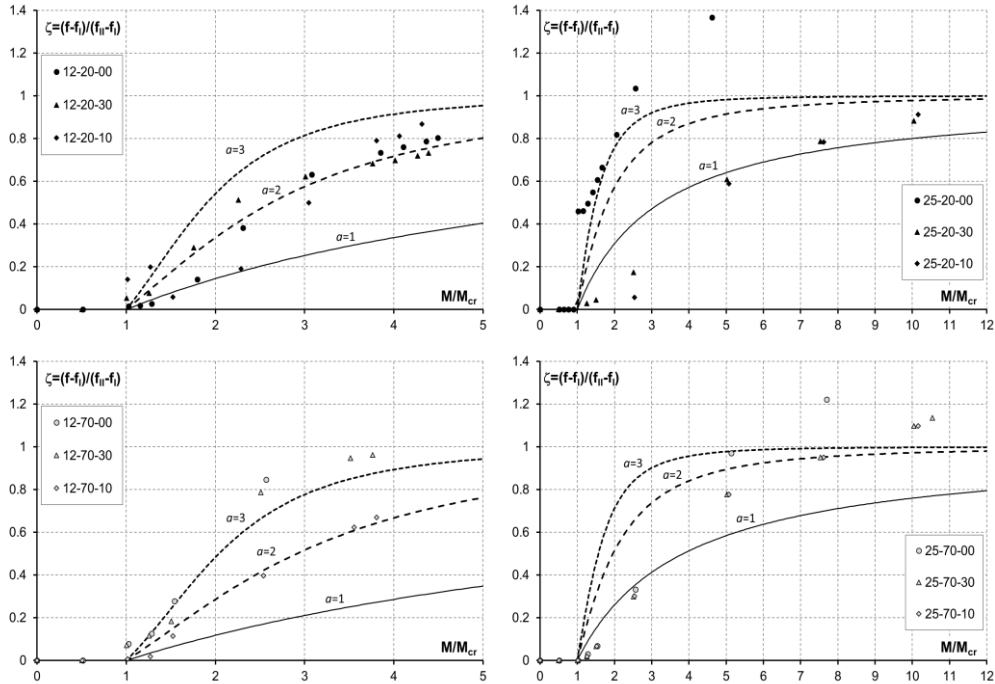


Fig. 19 Value of the interpolation coefficient ζ deduced from deflections and ACI (Branson) method

compared with measured deflections (f_{exp}). Rheological deflections produced by shrinkage of concrete are added using estimations in State II as commented previously (solving Equation (9)).

As can be seen, in general the values calculated are in the safe side, especially for lower loads levels, in which the results are clearly on the safe side. As the load is increased (higher deflections), the estimations and the measured deflections tend to be coincident. As commented previously, the scatter for relation $d/h = 0.80$ is important, reducing the accuracy of the estimations. However, the results obtained are sufficiently accurate for both situations.

Actually, the EC-2 and ACI methods have very similar curvature interpolation models. They

assume only a different power parameter a for the member M/M_{cr} , 2 and 3, respectively. Thus, the previous analysis carried out for EC-2 can be extended for ACI model. Thus, working in the same way that for EC-2 formulation, the power parameter a of Eq. 6 can be adjusted by least squares to the experimental data. To differentiate from the previous parameter defined for C-2, the power value is recalled here as a_B .

Fig. 19, similar to Fig. 16, present the comparison between the coefficient ζ , obtained from Equation 12 and the measured deflections, and the estimations obtained using Equation (6). Three values of the power parameter a_B are analysed: 1, 2 and 3 (actually, 3 is the value used by Branson method). Due the Branson methodology uses the inertial properties related to each section, the different families are presented separately.

In this case, the conclusion is not as evident as was previously for EC-2. The results demonstrates that the power parameter a_B changes not only with the concrete cover but also with on the amount of reinforcement. Besides, not always the value proposed by Branson overestimates the deflections obtained. For all these reasons, it is not possible to conclude a proposal for improvement of the actual Branson formulation.

8. Conclusions

In this paper an analytical-experimental study for deformation behaviour of beams has been carried out. This study, focused on short-term loads, has shown that some methods as EC-2 and Walraven approach fit better the experimental data of shrunk RC flexural elements. On the other hand, Branson approach and the methods proposed by Vecchio and Hsu fit better the experimental results after elimination of the shrinkage effect by the inverse methodology. In the case of steel related tension-stiffening law proposed by Model Code 2010, the underestimation can be significant when compared with free-of-shrinkage experimental results. As the reinforcement increases the difference between the accuracy of the different methods disappear due the reduction of tension-stiffening effect.

The interpolation coefficient ζ as specified by the EC-2 (as well as the Model Code) is used to analyse the accuracy of the actual codes. To include the ACI-318 normative, the Branson approach is adapted to obtain an estimation of ζ . The comparison of results has shown that Branson tends to underestimate the curvatures for elements with low reinforcement ratios (as slabs) and relations M/M_{cr} near to one (low load levels). This difference disappears for higher reinforcement ratios and load levels.

The exponential parameter a , used in EC-2 formulation to calculate the interpolation coefficient ζ , has been fitted to experimental results using a least squares approach in order to evaluate the accuracy of the actual value proposed by the normative ($a = 2$). The value of the exponent a , assessed on the basis of experimental data of shrunk elements, is found to be not less than 2.00. However, in case of analysing values of a obtained from “free-of-shrinkage” experimental data, it is observed a reduction of the power parameter respect to EC-2 proposal. It was found a good correlation between experimental and analytical results using $a = 1.00$ for $d/h = 0.92$ and $a = 1.50$ for $d/h = 0.80$. These estimations can be improved by adding an additional term which includes shrinkage effects based on the classical hypothesis of behaviour for State II. This allows to obtain an upper limit for the imposed curvatures.

Thus, from the results presented in this work it is shown that the existing empirical models deduced on the basis of test data of shrunk RC elements can be improved if the estimations are

carried out separately for short-term (inverse methodology) and shrinkage effects. In any case, given the limited size of the test sample analysed here more experimental campaigns are needed in order to validate the conclusions obtained in this paper.

Acknowledgements

The tests carried out at the Structures Laboratory of the Civil Engineering School of UPM were performed within the framework of the Research program lead by COMSA EMTE, S.A. with the participation of FHECOR Consulting Engineers and was partially funded by “Centro de Desarrollo Tecnológico Industrial” (CDTI) an organism of the Spanish Ministry of Science and Technology, under project number IDI-20080937.

The authors also wish to thank the Laboratory head José Torrico and visiting students from Politecnico di Milano, Francesco dal Pont and Andrea Facchini for their help in carrying out the tests.

Viktor Gribniak also wishes to acknowledge the support by the European Social Fund (Project Nr. 2013/0019/1DP/1.1.1.2.0/13/APIA/VIAA/062).

References

- ACI Committee 318 (2011), *Building Code Requirements for Structural Concrete and Commentary*, American Concrete Institute.
- Bach, C. and Graf, O. (1917), “Tests on reinforced concrete beams for obtaining moment-curvature relationships (Versuche mit Eisenbetonbalken zur Ermittlung der Beziehung zwischen Formänderungswinkel und Biegemoment)”, *Deutscher Ausschuss für Eisenbeton* (Bulletin N° 38). Berlin (in German).
- Balázs, G.L., Bisch, P., Borosnyói, A., Burdet, O., Burns, C., Ceroni, F. and Vráblík, L. (2013), “Design for SLS according to fib model code 2010”, *Struct. Concrete*, **14**(2), 99-123.
- Bazant, Z.P. (1972), “Prediction of concrete creep effects using age-adjusted effective modulus method”, *ACI J.*, 69(April), 212-217.
- Bazant, Z.P. and Oh, B.H. (1984), “Deformation of progressively cracking reinforced concrete beams”, *ACI Journal*, 81(May-June), 268-277.
- Bischoff, P.H. (2001), “Effects of shrinkage on tension stiffening and cracking in reinforced concrete”, *Can. J. Civ. Eng.*, **28**, 363-374.
- Bischoff, P.H. (2008), Discussion of “tension stiffening in lightly reinforced concrete slabs” by R. Ian Gilbert, *J. Struct. Eng.*, **133**(6), 1259-1260.
- Branson, D. (1963), “Instantaneous and time-dependent deflections of simple and continuous reinforced concrete beams HPR Report 7”, *Alabama Highway Department*, Bureau of Public roads.
- Branson, D. (1977), “Deformation of concrete structures”, McGraw-Hill, New York.
- CEB (1990), “Model Code 1990”, *Comité Européen du Béton*.
- CEB-FIP (2009), “Structural Concrete. Textbook on behaviour, design and performance. Second edition”, *International Federation for Structural Concrete (fib)*(Vol. 1, pp. 308), Lausanne, Switzerland.
- CEB-FIP (2012), “Model Code 2010. Final draft”, *International Federation for Structural Concrete (fib)*(Vol. 1, pp. 311), Lausanne, Switzerland.
- CEB-FIP (2012), “Model Code 2010. Final draft”, *International Federation for Structural Concrete (fib)*(Vol. 2, pp. 331), Lausanne, Switzerland.
- Collins, M.P., Mitchel, D., Perry, A. and Vecchio, F.J. (1996), “A general shear design method”, *ACI Struct.*

- J.*, **93**(1), 36-45.
- EC-2 (2004), "Eurocode-2: Design of concrete structures - Part 1-1: General rules and rules for buildings", *CEN. Brussels, B*.
- Ezeberry Parrotta, J.I. (2011), "Serviceability theoretical behaviour of RC members under external loads and imposed deformations (Comportamiento teórico de elementos de hormigón estructural en condiciones de servicio, sometidos a acciones exteriores y deformaciones impuestas)", MSc Thesis, *Polytechnic University of Madrid*, Madrid (in Spanish).
- Ghali, A., Favre, R. and Elbadry, M. (2012), "Concrete Structures. Stresses and Deformations: Analysis and Design for Service ability" (4 ed.), Spon Press. London, UK.
- Gilbert, R.I. (2001), "Shrinkage, cracking and deflection - the service ability of concrete structures", *Elect. J. Struct. Eng.*, **1**, 15-37.
- Gilbert, R.I. (2007), "Tension stiffening in lightly reinforced concrete slabs", *J. Struct. Eng.*, **133**(6), 899-903.
- Gilbert, R.I. (2008), Closure to "Tension stiffening in lightly reinforced concrete slabs", *J. Struct. Eng.*, **133**(6), 1264-1265.
- Gribniak, V. (2009), "Shrinkage influence of tension-stiffening of concrete structures" (PhD Thesis) *Vilnius Gediminas Technical University*, Vilnius, Lithuania. (<http://www.dart-europe.eu/full.php?id=182160>)
- Gribniak, V., Kaklauskas, G., Kacianauskas, R. and Kliukas, R. (2012), "Improving efficiency of inverse constitutive analysis of reinforced concrete flexural members", *Scientific Res. Essays*, **7**(8), 923-938.
- Gribniak, V., Kaklauskas, G., Torres, L., Daniunas, A., Timinskas, E. and Gudonis, E. (2013a), "Comparative analysis of deformations and tension-stiffening in concrete beams reinforced with GFRP or steel bars and fibers", *Composites: Part B*, **50**, 158-170.
- Gribniak, V., Cervenka, V. and Kaklauskas, G. (2013b), "Deflection prediction of reinforced concrete beams by design codes and computer simulation", *Eng. Struct.*, **56**, 2175-2186.
- Hsu, T.T.C. (1996), "Toward a unified nomenclature for reinforced-concrete theory", *J. Struct. Eng.*, **122**(3), 275-283.
- Kaklauskas, G. (2001), "Integral flexural constitutive model for deformational analysis of concrete structures", Monograph. Vilnius: Vilnius Technika.
- Kaklauskas, G. and Ghaboussi, J. (2001), "Stress-strain relations for cracked tensile concrete from RC beam tests", *J. Struct. Eng.*, **127**(1), 64-73.
- Kaklauskas, G. (2004), "Flexural layered deformational model of reinforced concrete members", *Mag. Concrete Res.*, **56**(10), 575-584.
- Kaklauskas, G., Gribniak, V. and Bacinskas, D. (2008), Discussion of "Tension Stiffening in Lightly Reinforced Concrete Slabs" by R. Ian Gilbert, *J. Struct. Eng.*, **113**(6), 1261-1262.
- Kaklauskas, G., Gribniak, V., Bacinskas, D. and Vainiunas, P. (2009), "Shrinkage influence on tension stiffening in concrete members", *Eng. Struct.*, **31**(6), 1305-1312.
- Kaklauskas, G. and Gribniak, V. (2011a), "Eliminating shrinkage effect from moment curvature and tension Stiffening relationships of reinforced concrete members", *J. Struct. Eng.*, **137**(12), 1460-1469.
- Kaklauskas, G., Gribniak, V. and Girdzius, R. (2011b), "Average stress-average strain tension-stiffening relationships based on provisions of design codes", *J. Zhejiang University-Science A*, **12**(10), 731-736.
- Kaklauskas, G., Gribniak, V., Salys, D., Sokolov, A. and Meskenas, A. (2011c), "Tension-Stiffening Model Attributed to Tensile Reinforcement for Concrete Flexural Members", Paper presented at the Twelfth East Asia-Pacific Conference on Structural Engineering and Construction.
- Perez Caldentey, A., Corres Peiretti, H., Petschke, T.P., Ezeberry Parrotta, J.I. and Giraldo Soto, A. (2012), "Serviceability design of columns of long jointless structures", *Eng. Struct.*, **44**, 359-371.
- Perez Caldentey, A., Corres Peiretti, H., Peset Iribarren, J. and Giraldo Soto, A. (2013), "Cracking of RC members revisited. Influence of cover, Φ/p_{eff} and stirrup spacing, An Experimental and Theoretical Study", *Struct. Concrete*, **14**(1), 69-78.
- Srinivasa Rao, P. and Subrahmanyam, B.V. (1973), "Trisegmental moment curvature relations for reinforced concrete", *ACI J. Proceedings*, **70**(5), 346-351.
- Trost, H. (1967), "Implications of the Superposition Principle in Creep and Relaxation Problems for

Concrete and Prestressed Concrete (Auswirkungen des Superpositionsprinzips auf Kriech- und Relaxationsprobleme bei Beton und Spannbeton)", *Beton-und Stahlbetonbau* (Berlin-Wilmersdorf), Heft 10, 230-238, 261-269 (in German).

Vecchio, F.J. and Collins, M.P. (1986), "The modified compression-field theory for reinforced concrete elements subjected to shear", *ACI J.*, **83**(2), 219-231.

Zanuy Sánchez, C. (2010), "Investigating the negative tension stiffening effect of reinforced concrete", *Struct. Eng. Mech.*, **34**(2), 189-211.

CC

Notation

ε	strain
ε_0	strain at the reference fibre Y_{ref}
ε_c	strain of concrete
ε_{cr}	strain of concrete for f_{ct}
ε_{cs}	shrinkage strain
ε_s	strain of steel
ζ	interpolation factor between States I and II
κ	curvature
κ_{cr}	cracking curvature
κ_{cs}	corrected cracking curvature
κ_{cs}^*	simplified curvature produced by shrinkage
κ_m	mean curvature
κ_I	curvature in State I
κ_{II}	curvature in State II
ρ	reinforcement ratio
χ	ageing coefficient
φ	creep coefficient
σ_c	stress in concrete
σ_s	stress in the reinforcement
θ_A, θ_B	rotation at supports A and B
$\Delta\theta_{AB}$	rotation difference between supports $\Delta\theta_{AB} = \theta_B - \theta_A$
$\Delta\theta_{cant,AB}$	rotation difference between cantilever ends
\varnothing	rebar diameter
a	exponential parameter which define the parameter ζ
A_c	concrete cross-section
A_s	reinforcement cross-section
A_{s1}	tensile reinforcement cross-section
A_{s2}	compressive reinforcement cross-section
b	width of the section
c	geometrical cover of longitudinal reinforcement ($c=h-d$)
d	effective depth of reinforcement

E_s	modulus of elasticity of steel
E_c	modulus of elasticity of concrete
E_{c0}	instantaneous modulus of elasticity of concrete
E_f	modulus of elasticity of the GFRP rebars
EA_h	Reference modulus (E_c) per homogenized cross-section area
EB_h	Reference modulus (E_c) per homogenized first moment of inertia
EI_h	Reference modulus (E_c) per homogenized second moment of inertia
EA_c	Reference modulus (E_c) per concrete cross-section area
EB_c	Reference modulus (E_c) per concrete first moment of inertia
f	vertical deflection (camber)
f_{cs}	vertical deflection produced by κ_{cs}^*
f_{cm}	mean compressive strength of concrete
f_{ct}	tensile strength of concrete
h	height of the cross section
I_g	moment of inertia for uncracked concrete section ignoring reinforcement
I_{II}	moment of inertia for the fully cracked section (State II)
L	beam span length
L_v	cantilever beam span length
M	bending moment
M_{cr}	cracking bending moment
N	axial force
RH	relative humidity
T	temperature
y	fibre location at cross section
Y_{ref}	reference fibre location

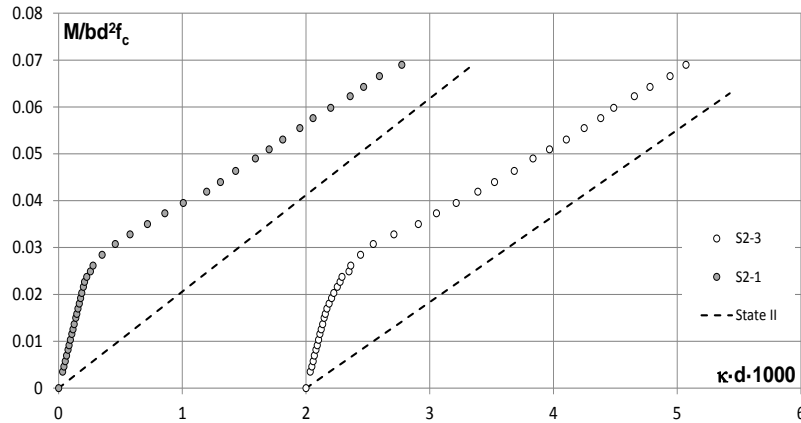


Fig. 20 Normalized experimental $M-\kappa$ relationships obtained by Gribniak *et al* (2013a). Fibre reinforced beams

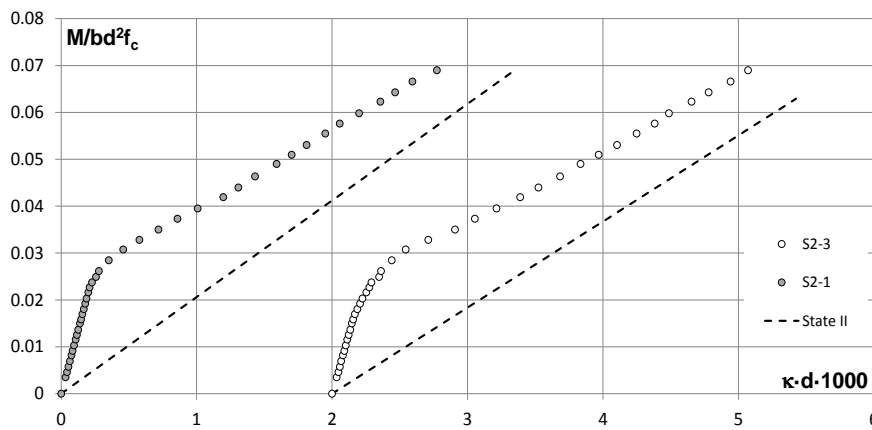


Fig. 21 Normalized experimental $M-\kappa$ relationships obtained by Gribniak *et al* (2013a). Steel reinforced beams

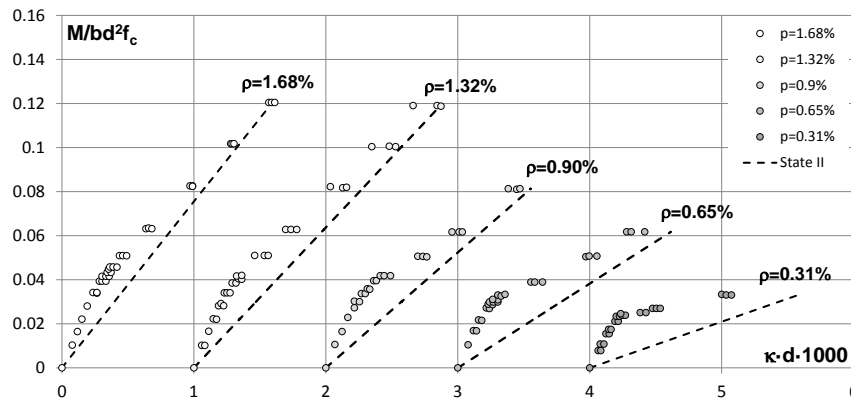


Fig. 22 Normalized experimental $M-\kappa$ relationships obtained by Bach and Graf (1917). Rectangular beams

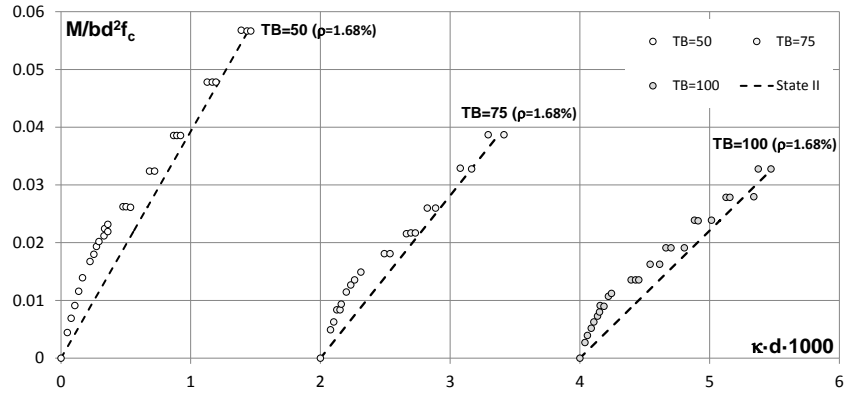


Fig. 23 Normalized experimental $M-\kappa$ relationships obtained by Bach and Graf (1917). T beams.